Inorganic Chemistry

Communication

pubs.acs.org/IC

# A Rational Strategy To Construct a Neutral Boron Imidazolate Framework with Encapsulated Small-Size Au−Pd Nanoparticles for Catalysis

De-Xiang Zhang, Juan Liu, Hai-Xia Zhang, Tian Wen,* and Jian Zhang*

State Key Laboratory of Structural Chemistry, Fujian Institute of Research on the Structure of Matter, Chinese Academy of Sciences, Fuzhou, Fujian 350002, P. R. China

Supporting Information

**ABSTRACT:** A series of 3D neutral boron imidazolate frameworks (BIFs) with octahedral metal centers were synthesized based on the charge-balancing principle. Au−Pd nanoparticles (NPs) with a mean size of 2.12 nm were then successfully obtained and encapsulated in these BIF structures through the simultaneous reduction of $Au^{3+}$/$Pd^{3+}$ ions by B−H bonds of tridentate boron ligands. The very small sizes of these Au−Pd NPs are attributed to the pore confinement effect of BIFs. This work not only brings new methodology for the construction of neutral BIFs but also suggests a new strategy for loading smaller-sized bimetallic NPs into BIFs.

Nowadays, functional porous materials like metal−organic frameworks (MOFs) have been explored dramatically because of their tentative applications in new sustainable development materials such as electrochemical energy storage devices and nanoparticle (NP)-incorporated catalysts.[1−7] As one newly developed type of MOFs, boron imidazolate frameworks (BIFs) present advantages similar to those of the well-developed hybrid zeolitic imidazolate frameworks (ZIFs) and pure inorganic zeolites. For the construction of ZIFs, a classic strategy is to connect $Zn^{2+}$ ions through imidazolate ligands to form 4-connected zeotype structures.[8−10] In the situation of BIFs, the most typical method is to combine $Cu^{+}$/$Li^{+}$ ions and presynthesized boron imidazolate ligands to mimic zeolite topologies (e.g., SOD and RHO).[11−13] Thus, the principle of charge balancing between metal ions and organic ligands is the key point for the construction of neutral BIFs and ZIFs. Considering this construction principle and the monocharge of boron imidazolate ligands, most of the reported BIFs are based on monovalent cations like $Cu^{+}$ and $Li^{+}$. However, in order to enrich the families of BIFs, it is urgent to find an efficient method to incorporate divalent metal cations into the BIF system.

To date, a number of NP-loaded MOFs have been successfully prepared and applied as catalysts for various reactions.[14−16] However, examples with MOFs as supporting host matrixes of bimetallic NPs are very rarely reported.[17] It still remains a great challenge to prepare bimetallic NP-functionalized porous materials with enhanced catalytic activities.

In our previous reports, a family of BIFs with interesting mechanochromic properties are synthesized using tetrahedral monovalent copper as the metal node.[18,19]Herein, we successfully developed a new strategy to construct neutral BIFs by combining divalent metal centers (e.g., $Zn^{2+}$/$Mn^{2+}$/$Cu^{2+}$/$Cd^{2+}$) and auxiliary ligand ($C_2O_4^{2-}$) to mimic the monovalent metal center [(+2) + $^1/_2$(−2) = (+1); Scheme 1]. With this rational idea, a series of block crystals of neutral BIFs (**BIF-39-Zn/Mn/Cu/Cd**) were synthesized through similar solvothermal reactions of $M^{2+}$, $B(im)_4^-$, and $C_2O_4^{2-}$ (Table 1). Single-crystal X-ray diffraction analyses indicate that the structures of these complexes are supramolecular isomers, which are formulated as $MB(im)_4{\cdot}0.5C_2O_4$ (M = Zn, Mn, Cu, Cd) and crystallize in a triclinic space group $P\bar{1}$. These crystalline samples are insoluble in common solvents (e.g., acetonitrile, water, and *N*,*N*-dimethylformamide). Furthermore, small Au−Pd bimetallic NPs with a mean size of 2.12 nm and exceptional catalytic stability were successfully loaded into **BIF-39-Cd** by applying $KBH(dm\text{-}bim)_3$ (dm-bim = 5,6-dimethylbenzimidazolate) as a moderate reductant.

**Scheme 1. Assembly Principle of Neutral BIFs between $B(im)_4^-$ and $[M^{2+}(^1/_2C_2O_4^{2-})]^+$**

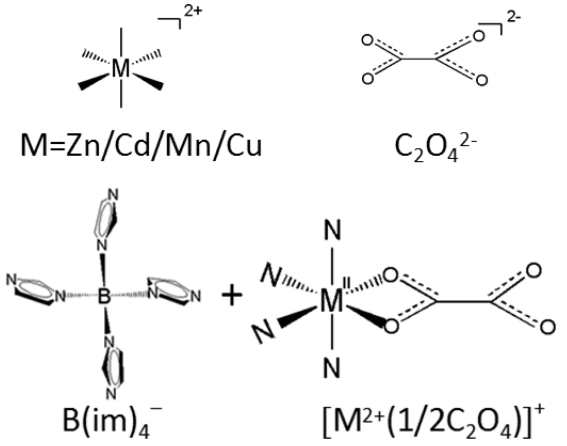


For convenience, **BIF-39-Cd** is selected as a representative and will be discussed in detail. The thermogravimetric behavior and phase purity of **BIF-39-Cd** have been demonstrated by thermogravimetric analysis (TGA) and powder X-ray diffraction (PXRD), respectively (Figures S1 and S2 in the Supporting Information, SI). In the structure of **BIF-39-Cd**, each $Cd^{2+}$ center is coordinated by four N atoms from four $B(im)_4^-$ ligands

**Received:** April 12, 2015
**Published:** June 18, 2015





DOI: 10.1021/acs.inorgchem.5b00826
*Inorg. Chem.* 2015, 54, 6069−6071

**Table 1. Summary of Crystal Data and Refinement Results**

| name | formula | space group | $a$ [Å] | $b$ [Å] | $c$ [Å] | $\alpha$ [deg] | $\gamma$ [deg] | $\beta$ [deg] | $V$ [Å$^3$] | R1 | wR2 |
|---|---|---|---|---|---|---|---|---|---|---|---|
| **BIF-39-Zn-a** | $ZnB(im)_4 \cdot 0.5C_2O_4$ | $P\bar{1}$ | 8.8017(4) | 10.6674(8) | 10.9422(8) | 103.157(6) | 108.193(6) | 97.410(5) | 927.91(11) | 0.0447 | 0.1376 |
| **BIF-39-Zn-b** | $ZnB(im)_4 \cdot 0.5C_2O_4$ | $P\bar{1}$ | 8.8649(4) | 10.5565(4) | 10.6310(5) | 99.986(3) | 99.986(3) | 97.819(4) | 898.42(7) | 0.0655 | 0.1813 |
| **BIF-39-Cu** | $CuB(im)_4 \cdot 0.5C_2O_4$ | $P\bar{1}$ | 8.7768(10) | 10.3933(9) | 11.0723(12) | 100.215(8) | 109.697(10) | 98.323(8) | 912.76(16) | 0.0472 | 0.1376 |
| **BIF-39-Cd** | $CdB(im)_4 \cdot 0.5C_2O_4$ | $P\bar{1}$ | 9.0162(7) | 10.7479(7) | 10.8068(4) | 97.570(4) | 97.708(5) | 110.100(6) | 956.61(10) | 0.0329 | 0.1070 |
| **BIF-39-Mn** | $MnB(im)_4 \cdot 0.5C_2O_4$ | $P\bar{1}$ | 8.9970(5) | 10.5163(5) | 10.6860(7) | 98.008(5) | 97.436(5) | 111.110(5) | 916.19(9) | 0.0389 | 0.1126 |

and two O atoms from an oxalate ligand, exhibiting an octahedral coordination geometry. The tetradentate $B(im)_4^-$ and oxalate ligands linked the six-coordinated and 5-connected $Cd^{2+}$ centers into a 3D framework with tcs topology (Figure 1d). Therein,

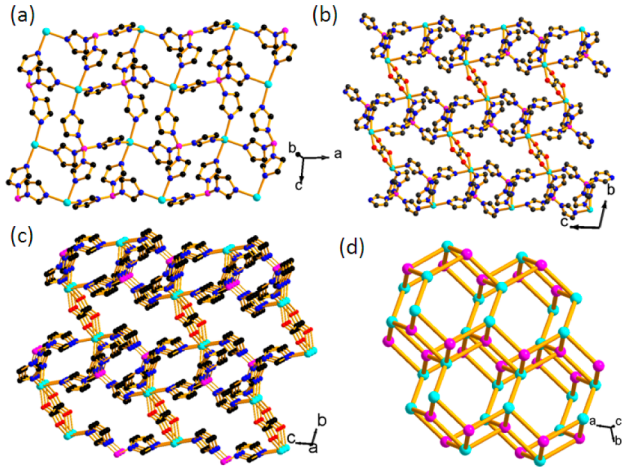


**Figure 1.** (a) View of a Cd−boron imidazolate layer without oxalate ligands. (b) View of 2D sheets linked into a 3D framework through $C_2O_4^{2-}$ pillars. (c) View of 3D packing of **BIF-39-Cd**. (d) View of tcs topology of **BIF-39-Cd**. Color code: Cd, pink blue; B, cyan; C, gray; N, blue. Partial H atoms are omitted for clarity.

$B(im)_4^-$ ligands connect $Cd^{2+}$ ions into a (4,4)-connected layer (Figure 1a). Also, the oxalate ligands further bridge the adjacent layers to form the 3D framework structure of **BIF-39-Cd** (Figure 1c). As a result, the oxalate ligands not only play a role in charge balancing but also act as linkers between two independent metal BIF units. The solvent-accessible void in **BIF-39-Cd** was 24%, as calculated by *PLATON* software.[20] Solvent molecules reside in the 1D channels along the *a* axis (Figure 1b).

According to our previous studies,[18,19,21−23] different sized metal NPs can be incorporated into BIFs by directly applying the rich active B−H bonds of tridentate boron imidazolate ligands as reducing agents. In the present study, considering the voids in these frameworks, we have extended this method to control the synthesis of noble metal Au−Pd NPs in the tetradentate BIFs. Here, in order to achieve better control over the synthesis of Au−Pd bimetallic NPs under mild conditions, $KBH(dm\text{-}bim)_3$ molecules were selected as reduction agents instead of $KBH_4$ and $NaBH_4$. A simple process was employed to prepare the **Au−Pd@BIF-39-Cd** sample. First, fresh **BIF-39-Cd** crystals (110 mg) were immersed in a mixed water solution of $HAuCl_4$ (20 mmol/L, 4 mL) and $HPdCl_4$ (20 mmol/L, 4 mL). Then the water solution of $KBH(dm\text{-}bim)_3$ (40 mmol/L, 4 mL) was added under stirring at room temperature to reduce $Au^{3+}$ and $Pd^{3+}$. After 6 h, an obvious color change of the crystals from pale yellow to brown was observed as a result of the loading of Au−Pd NPs into the crystals, indicating the formation of a **Au−Pd@BIF-39-Cd** sample (Figure S3 in the SI). The field-emission (FE) TEM images of the resulting **Au−Pd@BIF-39-Cd** sample indicate the formation of Au−Pd bimetallic NPs in the crystals (Figure 2a−

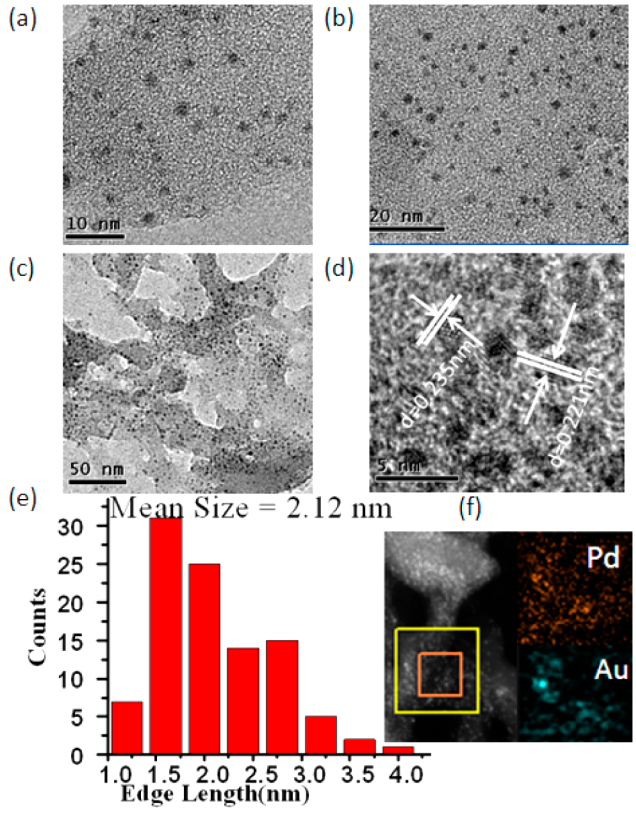


**Figure 2.** (a−c) Typical TEM images of the prepared **AuPd@BIF-39-Cd** with different magnifications. (d) HRTEM image of **AuPd@BIF-39-Cd**. (e) Particle-size distribution derived from TEM images, based on 100 randomly selected particles. (f) Mapping images of Pd and Au.

c). It can be seen that the application of $KBH(dm\text{-}bim)_3$ as reductants gave rise to Au−Pd bimetallic NPs with a narrow size distribution with an average size of 2.12 nm (Figure 2e). Moreover, the resulting Au−Pd bimetallic NPs also have a smaller size and more uniform distribution, compared with our group-reported metal−boron imidazolate systems whose framework structures are directly loaded NPs due to B−H fuctional bonds and even other groups of MOFs loading noble metal NPs.[18,19,21−24] The smaller size of the Au−Pd bimetallic NPs should be due to the moderate reductive ability of B−H bonds



DOI: 10.1021/acs.inorgchem.5b00826
*Inorg. Chem.* 2015, 54, 6069−6071

and also the pore confinement effect of the 1D channels in **BIF-39-Cd**, which could stabilize Au−Pd bimetallic NPs on the pore surface. In order to gain further information on the composition of **Au−Pd@BIF-39-Cd**, mapping images of Pd and Au (Figure 2f), energy-dispersive X-ray spectroscopy, and X-ray photoelectron spectroscopy (XPS) were used to characterize the samples (Figures S4 and S5 in the SI). The XPS spectrum of **Au−Pd@BIF-39-Cd** shows the binding energies of $Au^0$ (84 and 86 eV for $4f_{7/2}$ and $4f_{5/2}$, respectively) and $Pd^0$ (340 and 335 eV for $3d_{3/2}$ and $3d_{5/2}$, respectively). Moreover, the lattice fringe spacings of the Au−Pd bimetallic NPs were measured as 0.221 and 0.235 nm, which closely match the *d* values for Pd(111) and Au(111), respectively (Figure 2d). These results indicate the coexistences of $Au^0$, $Pd^0$, and $Cd^{2+}$ in the solid of **Au−Pd@BIF-39-Cd**. The PXRD patterns prove that the host framework of **BIF-39-Cd** is retained after the loading of Au−Pd bimetallic NPs. According to the above characterizations, it can be concluded that Au−Pd bimetallic NPs have successfully been incorporated into the phase of **BIF-39-Cd** crystals by using tridentate boron imidazolate molecules as reducing agents.

Further, the reduction of 4-nitrophenol by $NaBH_4$ was chosen as a model reaction for evaluating the catalytic performance of **Au−Pd@BIF-39-Cd**, which was monitored by UV−vis absorption spectroscopy. The UV−vis spectra show an isosbestic point, suggesting that they exhibit high catalytic activities (Figures S6 and S7 in the SI). TEM measurements indicate that the Au−Pd NPs did not change their sizes obviously after three runs. PXRD studies also reveal that the complex catalysts remain as their phase structures after catalytic experiments. Therefore, the **Au−Pd@BIF-39-Cd** catalyst not only shows good catalytic performance but also represents exceptional stability during catalysis (Figure S8 in the SI).

In summary, we have successfully designed and synthesized a new class of 3D neutral BIFs according to the valence balance principle. By the application of auxiliary $C_2O_4^{2-}$ ligands to reduce the charges of divalent metal to mimic the monovalent metal centers, $Zn^{2+}/Cu^{2+}/Mn^{2+}/Cd^{2+}$ ions have been successfully used as metal nodes for the construction of neutral BIFs. Our strategy opens new ways toward BIFs and will result in an explosive increase of these kinds materials. Moreover, we also successfully use tridentate boron imidazolates as mild reductants to simultaneously load Au−Pd NPs into BIFs. The moderate characteristics of the applied external reducing agents together with the pore confinement effect of the 1D channels cause the incorporated Au−Pd NPs to display smaller sizes than most of the reported metallic NPs@MOFs. Therefore, this work also provides new methodology for loading small bimetallic NPs into porous materials to form complex catalysts with good catalytic performances and high catalytic stabilities.

## ■ ASSOCIATED CONTENT

### Supporting Information

Experimental details, additional figures, TGA, PXRD patterns, and a CIF file (**BIF-39-Zn-a/b/Cu/Cd/Mn** CCDC 1057544−1057548). The Supporting Information is available free of charge on the ACS Publications website at DOI: 10.1021/acs.inorgchem.5b00826.

## ■ AUTHOR INFORMATION

### Corresponding Authors

*E-mail: twen@fjirsm.ac.cn.
*E-mail: zhj@fjirsm.ac.cn.

### Notes

The authors declare no competing financial interest.

## ■ ACKNOWLEDGMENTS

This work is supported by the 973 program (Grants 2011CB932504 and 2012CB821705) and the NSFC (Grants 21203196, 21221001, and 21425102).

## ■ REFERENCES

(1) Furukawa, H.; Cordova, K. E.; O'Keeffe, M.; Yaghi, O. M. *Science* **2013**, *341*, 1230444.
(2) Khan, I. A.; Haider, A. N.; Ullah, S.; Anjum, D. H.; Nadeem, M. A. *J. Solid State Electrochem.* **2014**, *18*, 1545−1555.
(3) Choi, K. M.; Jeong, H. M.; Park, J. H.; Zhang, Y.; Kang, J. K.; Yaghi, O. M. *ACS Nano* **2014**, *8*, 7451−7457.
(4) Lux, L.; Williams, K.; Ma, S. Q. *CrystEngComm* **2015**, *17*, 10−22.
(5) Zhu, Q. L.; Xu, Q. *Chem. Soc. Rev.* **2014**, *43*, 5468−5512.
(6) Gao, J.; Miao, J.; Li, P.-Z.; Teng, W. Y.; Yang, L.; Zhao, Y.; Liu, B.; Zhang, Q. *Chem. Commun.* **2014**, *50*, 3786−3788.
(7) Xiong, W.; Zhang, Q. *Angew. Chem., Int. Ed.* **2015**, DOI: 10.1002/anie.201502277.
(8) Huang, X. C.; Lin, Y.-Y.; Zhang, J. P.; Chen, X.-M. *Angew. Chem., Int. Ed.* **2006**, *45*, 1557−1559.
(9) Phan, A.; Doonan, C.; Uribe-Romo, F. J.; Knobler, C. B.; O'Keeffe, M.; Yaghi, O. M. *Acc. Chem. Res.* **2010**, *43*, 58−67.
(10) Li, K. H.; Olson, D. H.; Seidel, J.; Emge, T. J.; Gong, H. W.; Zeng, H. P.; Li, J. *J. Am. Chem. Soc.* **2009**, *131*, 10368−10369.
(11) Zhang, J.; Wu, T.; Zhou, C.; Chen, S.; Feng, P.; Bu, X. *Angew. Chem., Int. Ed.* **2009**, *48*, 2542−2545.
(12) Wu, T.; Zhang, J.; Zhou, C.; Wang, L.; Bu, X.; Feng, P. *J. Am. Chem. Soc.* **2009**, *131*, 6111−6113.
(13) Wu, T.; Zhang, J.; Bu, X.; Feng, P. *Chem. Mater.* **2009**, *21*, 3830−3837.
(14) Ke, F.; Zhu, J. F.; Qiu, L. G.; Jiang, X. *Chem. Commun.* **2013**, *49*, 1267−1269.
(15) Zhu, Q. L.; Li, J.; Xu, Q. *J. Am. Chem. Soc.* **2013**, *135*, 10210−10213.
(16) Chen, L. Y.; Peng, Y.; Wang, H.; Gu, Z. Z.; Duan, C. Y. *Chem. Commun.* **2014**, *50*, 8651−8654.
(17) Li, J.; Zhu, Q. L.; Xu, Q. *Chem. Commun.* **2014**, *50*, 5899−5901.
(18) Wen, T.; Zhang, D. X.; Liu, J.; Zhang, H. X.; Zhang, J. *Chem. Commun.* **2015**, *51*, 1353−1355.
(19) Wen, T.; Zhang, D. X.; Zhang, H. X.; Zhang, H. B.; Zhang, J.; Li, D. S. *Chem. Commun.* **2014**, *50*, 8754−8756.
(20) Spek, A. L. *Acta Crystallogr., Sect. A* **1990**, *46*, C34.
(21) Zhang, H. X.; Liu, M.; Bu, X.; Zhang, J. *Sci. Rep.* **2014**, *4*, 3923.
(22) Zhang, D. X.; Zhang, H. X.; Li, H. Y.; Wen, T.; Zhang, J. *Cryst. Growth Des.* **2015**, *15*, 2433−2436.
(23) Zhang, D. X.; Zhang, H. X.; Wen, T.; Zhang, J. *Dalton Trans.* **2015**, *44*, 9367−9369.
(24) Lim, D.-W.; Yoon, J.; Ryu, K. Y.; Suh, M. P. *Angew. Chem., Int. Ed.* **2012**, *51*, 9814−9817.



DOI: 10.1021/acs.inorgchem.5b00826
*Inorg. Chem.* 2015, 54, 6069−6071